

The Spatial Distribution of Galactic Satellites in the Λ CDM Cosmology

Jie Wang¹ *, Carlos S. Frenk¹ and Andrew P. Cooper²

¹*Institute for computational cosmology, Department of Physics, University of Durham, South Road, Durham, DH1 3LE, UK*

²*Max-Planck-Institut für Astrophysik, Karl-Schwarzschild-Str. 1, D-85748 Garching, Germany*

Accepted 2012 ???? ?. Received 2012 ???? ?; in original form 2007 ???? ?

ABSTRACT

We investigate the spatial distribution of galactic satellites in high resolution simulations of structure formation in the Λ CDM model: the Aquarius dark matter simulations of individual halos and the Millennium II simulation of a large cosmological volume. To relate the simulations to observations of the Milky Way we use two alternative models to populate dark halos with “visible” galaxies: a semi-analytic model of galaxy formation and an abundance matching technique. We find that the radial density profile of massive satellites roughly follows that of the dark matter halo (unlike the distribution of dark matter subhalos). Furthermore, our two galaxy formation models give results consistent with the observed profile of the 11 classical satellites of the Milky Way. Our simulations predict that larger, fainter samples of satellites should still retain this profile at least up to samples of 100 satellites. The angular distribution of the classical satellites of the Milky Way is known to be highly anisotropic. Depending on the exact measure of flattening, 5–10 per cent of satellite systems in our simulations are as flat as the Milky Way’s and this fraction does not change when we correct for possible obscuration of satellites by the Galactic disk. A moderate flattening of satellite systems is a general property of Λ CDM, best understood as the consequence of preferential accretion along filaments of the cosmic web. Accretion of a single rich group of satellites can enhance the flattening due to such anisotropic accretion. We verify that a typical Milky Way-mass CDM halo does not acquire its 11 most massive satellites from a small number of rich groups. Single-group accretion becomes more likely for less massive satellites. Our model predictions should be testable with forthcoming studies of satellite systems in other galaxies and surveys of fainter satellites in the Milky Way.

Key words:

1 INTRODUCTION

The satellites of the Milky Way offer a number of critical tests of the current cosmological paradigm, the Λ CDM model. Their abundance and internal structure are sensitive to the nature of the dark matter and thus to the high frequency end of the linear power spectrum of density fluctuations. Their spatial distribution is sensitive to the gravitational evolution of dark matter on galactic and supergalactic scales.

High resolution simulations of the formation of galactic cold dark matter halos have revealed that a large number of substructures survive to the present day, accounting for about 10% of the total halo mass (Diemand et al. 2007; Springel et al. 2008, and references therein). Since

only about two dozen satellites are known to orbit in the halo of the Milky Way, this property is frequently deemed to pose a “satellite problem” for CDM-based cosmologies. In fact, it was shown about a decade ago that basic processes that are unavoidable during galaxy formation, such as supernova feedback and early Hydrogen reionization, readily explain why a visible satellite galaxy can form only in a tiny fraction of the surviving subhalos (Bullock et al. 2000; Benson et al. 2002; Somerville 2002). This result has been confirmed repeatedly in recent years using semi-analytic models (Cooper et al. 2010; Guo et al. 2011; Li et al. 2010; Macciò et al. 2010; Font et al. 2011), cosmological gas-dynamical simulations (Okamoto et al. 2010; Parry et al. 2012; Wadepuhl & Springel 2011) and simplified semi-empirical models (Kravtsov et al. 2004; Koposov et al. 2009; Busha et al. 2010; Muñoz et al. 2009).

A different kind of theoretical challenge is posed by the

* Email: jie.wang@durham.ac.uk

spatial distribution of the 11 classical satellites of the Milky Way. Lynden-Bell (1976), Kunkel (1979) and Lynden-Bell (1982) noted that these satellites lie very close to a great circle on the sky that is approximately perpendicular to the Galactic Plane. Kroupa et al. (2005) deemed such a highly flattened structure to be extremely unlikely in a CDM cosmology but, using N-body simulations of halo formation in the Λ CDM model, Kang et al. (2005), Libeskind et al. (2005), Zentner et al. (2005) and Libeskind et al. (2009) showed explicitly that this presumption is incorrect. Such flattened satellite distributions were dubbed “great pancakes” by Libeskind et al. (2005) who ascribed them to highly anisotropic accretion of proto-subhalos along the filaments of the cosmic web. Correlated accretion along filaments was also identified as the cause for the polar alignment of satellite disks found by Deason et al. (2011) in 20 percent of satellite systems (with more than 10 bright members each) in the “GIMIC” N-body/gasdynamical simulations (Crain et al. 2009). Although all of these studies found that flattening of satellite systems is common in Λ CDM, they also found that the high degree of flattening in the Milky Way system is atypical.

Li & Helmi (2008) showed that the flattening effects of anisotropic accretion are greatly enhanced in cases where infalling dark matter subhalos belong to a ‘group’ sharing similar infall times and orbital angular momentum orientations (the members of such groups do not have to be bound in a single DM halo before infall). In a Milky Way-mass system, they found that samples of ~ 10 subhalos drawn from one or two such groups readily produced configurations as flat as that of the classical Milky Way satellites. Extrapolating this result, they suggested that the highly correlated infall of a rich group of satellites was a *possible* explanation for the abnormal degree of flattening seen in the Milky Way. However, they could not say whether this was a *probable* explanation since they did not calculate the likelihood of all the 11 *brightest* satellites being members of only one or two such groups.

An important limitation of the simulations that have been analysed so far to study the spatial distribution of satellites is their relatively low resolution. Low resolution can give rise to excessive tidal disruption and to the artificial merging of some subhalos, potentially obscuring the true spatial distribution. In this paper, we use the suite of six simulations of individual Galactic halos from the Aquarius project, which are amongst the highest resolution CDM simulations carried out to date (Springel et al. 2008), as well as a sample of similar halos from the Millennium-II simulation (Boylan-Kolchin et al. 2009). Millennium-II has lower resolution than Aquarius but follows halo formation in a cosmological volume (a cube of side $100 h^{-1} \text{Mpc}$, where h denotes the Hubble constant in units of $100 \text{ km s}^{-1} \text{Mpc}^{-1}$). With the Aquarius simulations we are able to study satellites down to very small masses in six galactic halos and with the Millennium-II we are able to study the massive satellites of a large sample of galactic halos. Since the Aquarius halos are zoom-resimulations of regions in the Millennium-II volume, we are able also to study the effects of numerical resolution.

We rank satellites in our simulations by stellar mass using two different techniques: semi-analytic modelling and a simple assignment of the brightest satellites to the most

massive proto-subhalos. As we show, the two approaches pick out similar subsets of subhalos as satellite hosts. With these samples, we revisit the radial distribution of satellites and the great pancake and, for the first time, we investigate how these properties depend on the number of satellites considered (in samples ranked by stellar mass). This allows us to make predictions for forthcoming surveys such as Pan-STARRS (Kaiser et al. 2010), which may discover a large population of very faint satellites in the Milky Way and M31, and the ongoing PANDAS survey of M31 (McConnachie et al. 2009; Martin et al. 2009). We also extend the work of Li & Helmi (2008) by using Aquarius to investigate the multiplicity function of groups of massive satellites.

The paper is organized as follows. In Section 2, we discuss the suite of simulations and galaxy formation models that we use. In Section 3, we investigate the radial distribution of satellites, the prevalence of great pancakes, and groups of massive satellites. Our conclusions and discussion are presented in Section 4.

2 SATELLITE IDENTIFICATION

We begin by providing a brief introduction to the Aquarius and Millennium-II simulations and then describe the two alternative techniques we have employed to identify satellites in them.

2.1 Aquarius and Millennium II

The Aquarius Project (Springel et al. 2008) consists of a suite of very high resolution N-body simulations of six dark matter halos of mass similar to that expected for the halo of the Milky Way. The simulations assume the Λ CDM cosmology, with parameters consistent with the WMAP 1 data (Spergel et al. 2003): matter density parameter, $\Omega_M = 0.25$; cosmological constant term, $\Omega_\Lambda = 0.75$; power spectrum normalization, $\sigma_8 = 0.9$; spectral slope, $n_s = 1$; and Hubble parameter, $h = 0.73$. These values are inconsistent with the WMAP 7 data at about the 2σ level, but this discrepancy is of no consequence for the analysis of this paper (see Wang et al. 2012).

The six Aquarius halos are labelled “Aq-A” through “Aq-F”. Each was resimulated at different resolution in order to assess numerical convergence. A suffix 1 to 5 identifies the resolution level, with level 1 denoting the highest resolution. In this study, we analyse primarily the level 2 simulations. For the level 2 simulations, the particle mass is $m_p \simeq 1 \times 10^4 h^{-1} M_\odot$ and the softening length is $\epsilon = 48 h^{-1} \text{pc}$. At $z = 0$, the six halos have a “virial” mass, $M_{200} \sim 1\text{--}2 \times 10^{12} h^{-1} M_\odot$, where M_{200} is the mass contained within r_{200} , the radius of a sphere of mean density 200 times the critical density for closure. The circular velocity curves of the halos peak at $V_{\text{max}} = 220 \pm 40 \text{ km s}^{-1}$. Although the Aquarius halos have similar final masses, they have varied formation histories (Wang et al. 2011). For further details of the Aquarius Project, we refer the reader to Springel et al. (2008) and Navarro et al. (2010).

At every snapshot in the simulations we find nonlinear structures using the friends-of-friends (FOF) algorithm of Davis et al. (1985), with a linking length of 0.2 times the

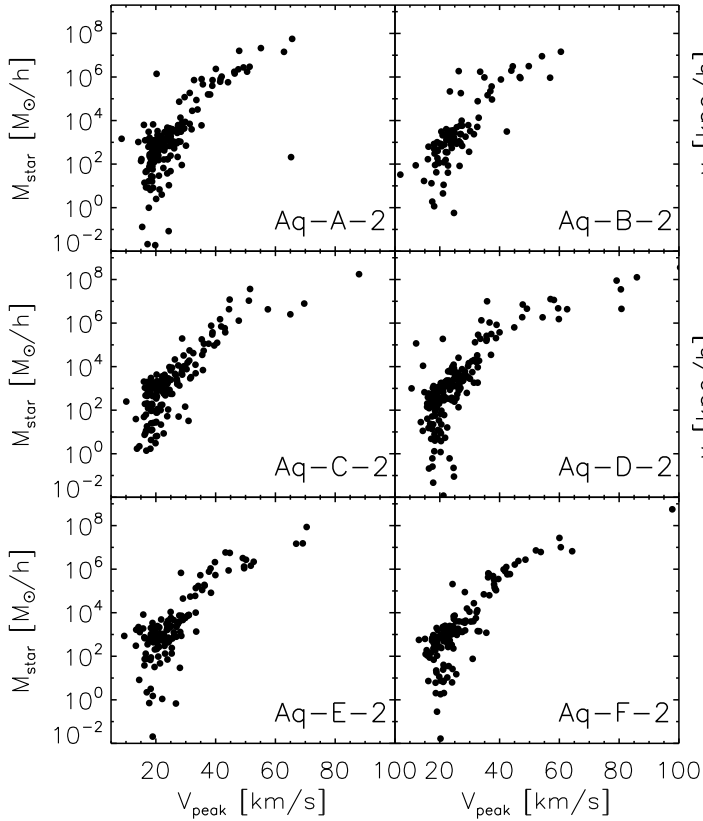


Figure 1. The relationship between the stellar mass assigned by the Cooper et al. (2010) semi-analytic model to subhalos in the six Aquarius simulations and the maximum value of the rotation curve attained by each subhalo over its entire past history. (Satellites with unresolved dark matter haloes are excluded.) The tight correlation for the most massive satellites motivates a simple V_{peak} model for ranking satellites by stellar mass.

mean interparticle separation and 32 particles as the minimum number of particles per group. We also identify bound substructures within each FOF halo using the SUBFIND algorithm of Springel et al. (2005). Merger trees for subhalos are constructed as described in Springel et al. (2008).

The Millennium-II run (MII) is a cosmological simulation in which 2160^3 particles were followed in a cubic box of side length $L_{\text{box}} = 100 \text{ Mpc } h^{-1}$. This volume is 125 times smaller than that of the Millennium simulation (Springel et al. 2005), and the mass resolution is correspondingly 125 times better: each particle has mass $6.88 \times 10^6 h^{-1} M_{\odot}$. The cosmological model is the same as that assumed for the Aquarius Project. For further details, we refer the reader to Boylan-Kolchin et al. (2009).

The Aquarius halos are resimulations of regions selected from a low resolution version of the MII with identical large-scale density perturbations and phases in their initial conditions. We can therefore find the counterparts of each Aquarius halo in the MII and carry out resolution tests (see

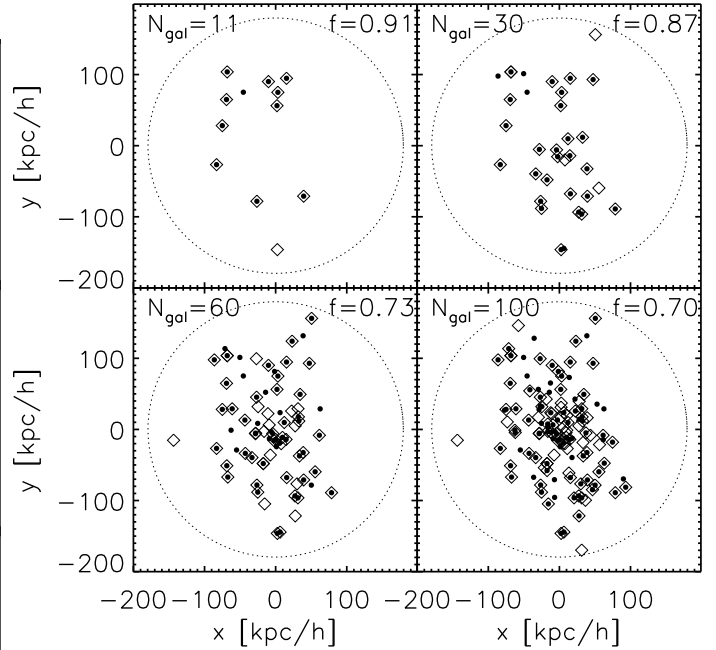


Figure 2. The projected positions of satellites identified using the Cooper et al. (2010) semi-analytic model (diamonds) and the V_{peak} method (filled circles) in the Aq-A2 halo. From top left to bottom right, positions are shown for the top 11, 30, 60 and 100 satellites ranked by stellar mass in each model. The overlap ratio between the two samples is given in the legend. It decreases from $f = 0.91$ for the top 11 to $f = 0.7$ for the top 100 satellites.

Boylan-Kolchin et al. 2009). The resolution of the MII is similar to that of the simulations analysed by Kang et al. (2005) and Zentner et al. (2005), but it is a factor of ~ 30 worse than the simulation by Libeskind et al. (2005) and a factor of ~ 20 better than that by Libeskind et al. (2009).

2.2 Galaxy formation models

There are two techniques for modelling satellite galaxies in detail using simulations: direct hydrodynamic simulations and semi-analytic modelling applied to a high-resolution N-body simulation of the dark matter. The two techniques are similar, differing primarily in the simplified, spherically symmetric treatment of gasdynamics in the semi-analytic method. In this study, we are interested in very faint satellites. Even the highest resolution gasdynamic simulations of satellites performed to date (Okamoto et al. 2010; Wadepuhl & Springel 2011) can resolve only the dozen or so brightest galaxies of a Milky Way system and so they are not suitable for our purposes. Semi-analytic models, on the other hand, are restricted only by the resolution of the associated N-body simulation so we resort instead to the semi-analytic models applied to the Aquarius simulations by Cooper et al. (2010) and to the MII by Guo et al. (2011). We refer the reader to these papers for details of the implementation. An added advantage of the semi-analytic models is that, unlike

the direct gasdynamic simulations, these models are known to agree with a whole range of other properties of the galaxy population at various epochs.

In practice, despite the complexity of the many physical processes they incorporate, both gasdynamic and semi-analytic simulations predict an approximately monotonic relation between the stellar mass of a galaxy and the total mass of the halo in which it forms. As we are only interested in the stellar mass rank of satellites, it is instructive to consider a much simpler model for satellites in which the stellar mass (hence luminosity) of each satellite is assumed to be proportional to the highest value of the maximum of the circular velocity curve (V_{\max}) attained by the halo in which the satellite forms throughout its entire history. We denote this by V_{peak} ; it corresponds roughly to the value of V_{\max} just prior to the halo being accreted into the main halo and becoming a subhalo. We refer to this as the “ V_{peak} model”. By comparing our semi-analytic results with this simpler but fundamentally similar model, we can check if our conclusions depend on the details of the semi-analytic treatment, which introduces a scatter in the relationship between stellar mass and (maximum) halo mass.

The correspondence between V_{peak} and M_{star} , the stellar mass of the semi-analytic model of Cooper et al. (2010), is illustrated in Fig. 1. The expected monotonic relation is apparent. However, there is considerable scatter in the relation for subhalos with $V_{\text{peak}} \lesssim 25 \text{ km s}^{-1}$. At higher masses, in the range of the 11 classical satellites, the relation flattens and the scatter is greatly reduced. In this regime, over 90% of the satellites with the highest V_{peak} values also have the highest M_{star} according to the semi-analytic model. Fig. 1 shows that our simple V_{peak} model will give a ranking of subhalos by stellar mass very similar to that of the semi-analytic model, in most cases.

The internal structure of halos that are close to the resolution limit of an N-body simulation is, of course, poorly modelled. This can lead to the artificial disruption of these halos when they are accreted into larger halos. The baryonic properties of their associated galaxies can still be followed in semi-analytic models even after the subhalos fall below the resolution of the simulation, but as their orbits cannot be tracked within the N-body simulation their spatial distribution is uncertain and model-dependent. The resolution of the Aquarius simulations is so high that we need not worry about galaxies with unresolved haloes (see discussion of this point in Font et al. 2011). However, at the lower resolution of the MR II, galaxies in unresolved haloes do need to be taken into account, as discussed by Guo et al. (2011). This conclusion is supported by our investigation of the radial distribution of satellites in MR II in the following section. We demonstrate that convergence with Aquarius is only possible if we include galaxies without resolved subhaloes in the Guo et al. model. In addition, because the circular velocity scale corresponding to the V_{peak} of the most massive satellites ($30\text{--}60 \text{ km s}^{-1}$) is close to the resolution limit of MR II, we can only make reliable comparisons between the semi-analytic and the V_{peak} models in the Aquarius simulations, and not in the MR II.

In Fig. 2 we compare the projected positions of the top 11, 30, 60, and 100 satellites ranked by stellar mass in Aq-A-2 according to the semi-analytic model (diamonds) and the V_{peak} method (full circles). As we can see in the top-left

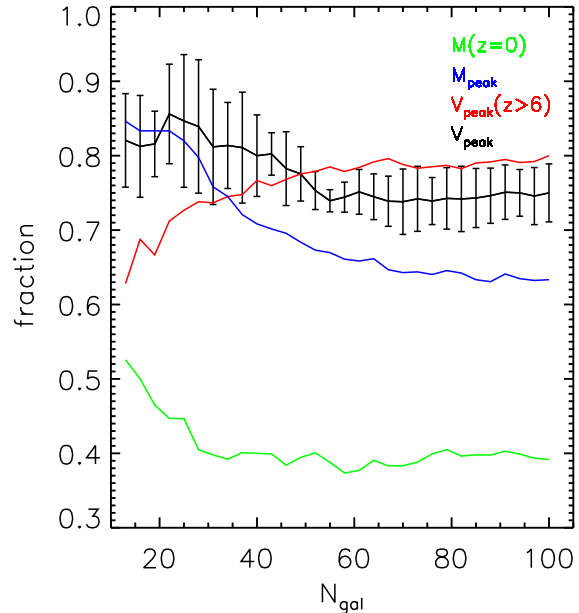


Figure 3. The fraction of satellites ranked according to different criteria that overlap with the top N_{gal} satellites ranked according to the stellar mass assigned to them by the Cooper et al. (2010) semi-analytic model. The data correspond to the mean value for all six Aquarius halos. The black line shows the overlap with our standard V_{peak} model and the 1σ error bar obtained from the 6 Aquarius simulations. The green line shows the result of ranking satellites according to their present mass and the blue line according to the maximum mass ever attained by the halo in which they reside today. The red line is similar to the V_{peak} model, except that in this case V_{peak} is defined as the maximum value attained by V_{\max} before $z = 6$, approximately the redshift of reionization.

panel, 10 out of the top 11 satellites are the same in both models, an overlap ratio, $f = 10/11 = 0.91$. As we consider smaller and more numerous satellites, f decreases, but even for the top 100 satellites, f is still as high as 70 percent.

In Fig. 3 we compare the overlap fractions between the top n_{gal} satellites ranked according to the stellar mass assigned by the Cooper et al. (2010) model and various simplified but plausible models for identifying satellites with subhalos, including our standard V_{peak} model (black line with error bars). The overlap fraction for the V_{peak} model tends to a constant, $f \simeq 0.75$, for $n_{\text{gal}} \gtrsim 60$. The green line corresponds to the case in which satellites are identified with the most massive subhalos at the present day (Stoehr et al. 2002). Clearly, this method fails to place satellites in similar subhalos to those picked out by our two standard models. The reason for this is simply that the present mass of a subhalo is significantly affected by tidal stripping and thus is only weakly correlated with the mass of the halo prior to accretion, during which time most of the satellite stars form.

Identifying satellites instead with subhalos ranked by the maximum mass they ever attain (blue line) gives a better match to the standard models since this mass is better correlated with the satellite’s stellar mass or luminosity. Even in this case, though, the overlap falls to just over 60 percent

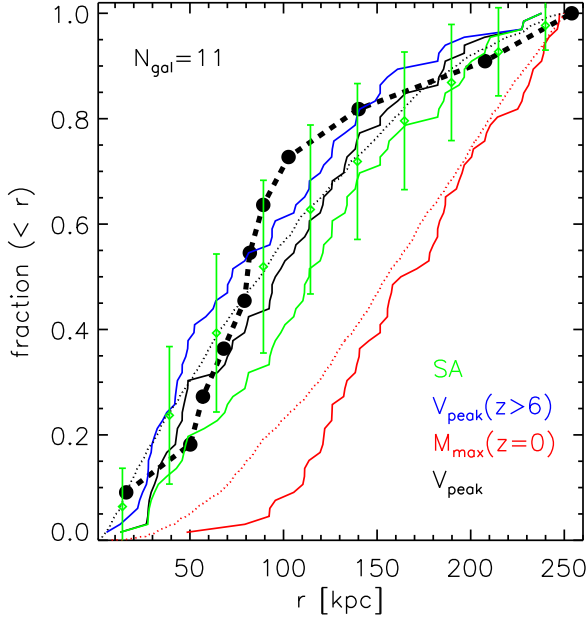


Figure 4. The radial profiles of the top 11 satellites in different models. Results have been averaged over the 6 Aquarius halos. The profile of the 11 classical satellites of the Milky Way is shown by the filled circles joined with a thick dashed black curve. The radial profile of the dark matter is shown by the black dotted curve and the radial profile of all resolved subhalos in the six Aquarius halos by the red dotted curve. The green, blue, red and black lines show the distribution of satellites in the Aquarius simulations, identified using different models, as indicated in the legend. The green diamonds with error bars correspond to satellites in the semi-analytic model applied to the MR11, including satellites without resolved dark matter haloes.

for large satellite populations. The red line shows what happens if we identify satellites according to the value of V_{peak} attained prior to $z = 6$, roughly the redshift of reionization. This model gives similar results to our standard V_{peak} model, except for the most massive satellites, reflecting, in part, the fact that reionization plays a relatively minor role in setting the stellar mass of these galaxies (see e.g. Okamoto et al. 2010; Font et al. 2011). We conclude that our choice of V_{peak} is the most appropriate of these alternatives and in most of the remainder of this paper we focus on comparisons between satellites ranked by this property and by the stellar mass in our semi-analytic models.

3 RESULTS

In this section we consider the spatial distribution of satellite galaxies predicted in both our semi-analytic and V_{peak} models and compare them with data for satellites in the Milky Way.

3.1 Radial profiles

The radial distribution of the 11 classical satellites of the Milky Way is shown by the filled circles in Fig. 4. The Galac-

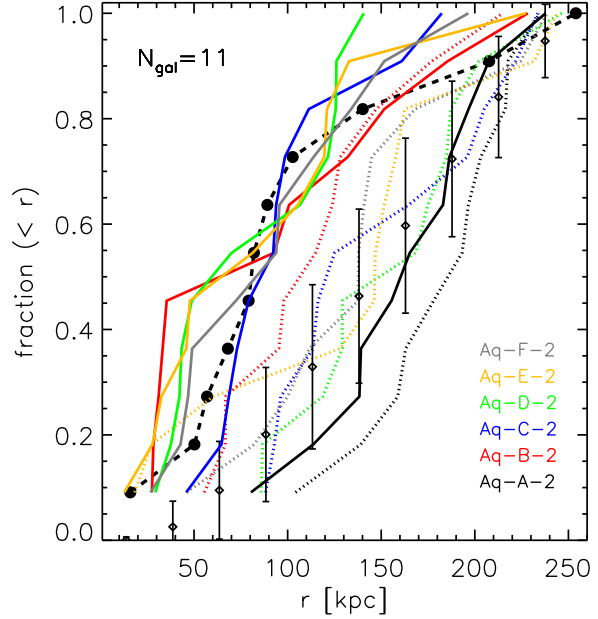


Figure 5. The radial profile of the 11 brightest satellites according to the V_{peak} model in each of the six Aquarius halos (solid lines) and in their counterparts in the MR11 (dotted lines). The diamonds and large error bars correspond to the average profile and 1σ dispersion of the top 11 satellites identified by the V_{peak} model in 1686 MR11 halos of mass $1 \times 10^{12} M_{\odot} < M_{200} < 2 \times 10^{12} M_{\odot}$. The profile of the 11 classical Milky Way satellites is shown by the black circles joined with a dashed black curve.

to-centric distance used here is taken from Mateo (1998). It is close to the radial distribution of the dark matter in the Aquarius halos, shown in the figure by the black dotted line, a similarity already noted by Kang et al. (2005), Libeskind et al. (2005) and Font et al. (2011). To compare the data to our models, we select the top 11 satellites in each model that lie within a distance of 250 kpc from the centre of the halo, roughly the distance of Leo I, the most distant of the observed Milky Way eleven.

Results for the semi-analytic, V_{peak} , $V_{\text{peak}}(z > 6)$ and $M_{\text{max}}(z = 0)$ models are shown by the green, black, blue and red solid lines respectively. All, except the last, are roughly consistent with the data within the large uncertainties due to small number statistics (see also Cooper et al. 2010; Font et al. 2011). By contrast, identifying satellites with the most massive present day subhalos (red line) leads to a much more extended distribution which, as first noted by Libeskind et al. (2005), closely follows the radial profile of the entire halo population. This is consistent with the finding by Springel et al. (2008) that the radial profile of subhalos depends very weakly on subhalo mass. The other, more realistic, models place bright satellites in subhalos whose radial profiles are strongly biased relative to that of the subhalo population as a whole and which happen to lie close to the dark matter radial profile. We also show results for Milky Way galaxies from the semi-analytic model applied to the MR11, taking care to include satellites which survive even though their dark matter halos have been tidally stripped.

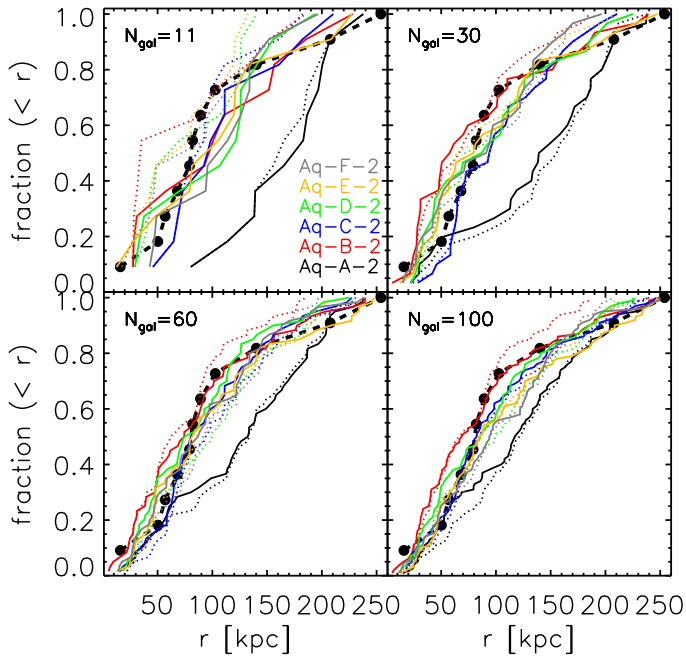


Figure 6. The cumulative radial profiles of the top N_{gal} satellites in each of the Aquarius halos in the semi-analytic (solid lines) and V_{peak} (dotted lines) models. The profile of the 11 classical satellites of the Milky Way is shown in all panels by the solid dots joined by a thick dashed black curve.

The distribution is close to the observational data. However, had we not included satellites without resolved dark matter halos, the profile would lie close to that of all subhaloes (red dotted).

The model lines in Fig. 4 are smoother than the Milky Way data because we averaged the distributions of the 11 top-ranked satellites from each of the 6 Aquarius halos. There is, in fact, considerable halo to halo scatter, as may be seen in Fig. 5, which shows the radial profiles of the 11 brightest satellites predicted by the semi-analytic model in each halo. Five of these lie very close to the Milky Way data but in Aq-A, the radius enclosing half the satellites is over twice as large as in the other 5 Aquarius halos.

Fig. 5 also highlights the importance of high resolution simulations for this kind of study. Since the Aquarius halos were selected from the M_{RII}, we can identify their counterparts in that simulation, as described by Boylan-Kolchin et al. (2010). The radial profiles of the top 11 satellites in these counterparts, as identified in the V_{peak} model, are shown by the dotted lines in the figure, with colours corresponding to those of the Aquarius halos. Satellites in the M_{RII} counterparts are clearly much more extended than the Aquarius subhalos. This is typical of the satellite distributions in Milky Way-mass halos in the M_{RII}, as illustrated by the diamonds with error bars, obtained by averaging the distributions of the 11 brightest satellites in the 1686 M_{RII} halos of mass $1 \times 10^{12} \leq M_{200} \leq 2 \times 10^{12}$. The M_{RII} has about 1000 times lower resolution than the

level 2 Aquarius simulations. As a result, subhalo orbits are not followed as accurately and their disruption timescale is artificially reduced.

The semi-analytic model of Guo et al. (2011) allows galaxies to survive after their host subhalo falls below the resolution limit. A position is assigned to these galaxies by tracking the most-bound particle of the host subhalo from the time it was last resolved. This position is unlikely to be a very accurate estimate of the true orbit of the satellite; for example, Guo et al. make an analytic correction to this single-particle orbit when calculating the tidal disruption of the satellite, as the orbits of individual particles do not decay through dynamical friction in an N-body simulation. Nevertheless, when we include satellites with unresolved haloes in our top 11 sample, as was done in Fig. 4 (but *not* in Fig. 5), and use their single-particle position estimates, the M_{RII} radial profiles for the Aquarius galaxies are in reasonable agreement with their higher resolution counterparts.

As we expect that larger and more complete samples of fainter satellites will soon be available for the Milky Way and other galaxies, it is interesting to know how the radial profiles of satellites are predicted to vary with the luminosity cut of the sample. This is a question that we can address with the Aquarius simulations and we do this in Fig. 6, where we show the radial profiles of the top 11, 30, 60 and 100 galaxies predicted in the semi-analytic (solid curves) and V_{peak} (dotted curves) models. The profiles depend only weakly on the size of the sample within the mass range we can examine: they are all similar to that of the 11 classical satellites of the Milky Way. The exception is Aq-A whose profiles become increasingly less discrepant with the other 5 Aquarius cases as the satellite sample size increases (although it is still the least concentrated even when 100 satellites are considered). By most other measures Aq-A is representative of haloes of the same mass (Boylan-Kolchin et al. 2010), suggesting that the top 11 satellites may often exhibit ‘unusual’ configurations in otherwise ‘typical’ haloes.

3.2 The angular distribution of satellites and the great pancake

As we have seen in the preceding section, the semi-analytic and V_{peak} models reproduce the observed radial profile of the 11 classical satellites of the Milky Way. In this subsection we investigate if they also reproduce the highly flattened configuration seen in the Milky Way, first noted by Lynden-Bell (1976) and investigated more recently by Kroupa et al. (2005); Libeskind et al. (2005); Kang et al. (2005); Libeskind et al. (2009) and Deason et al. (2011). We use similar techniques to those introduced by Libeskind et al. (2005) and Kang et al. (2005) to describe the flattening of the satellite population, namely, the overall shape of its distribution and its thickness in the flattest dimension.

3.2.1 The axis ratios of satellite systems

To determine the shape of a satellite system we calculate the moment of inertia tensor of its members (weighting each of them equally) and derive the principal axes of the distribution. The eigenvalues of the diagonalised inertia tensor are

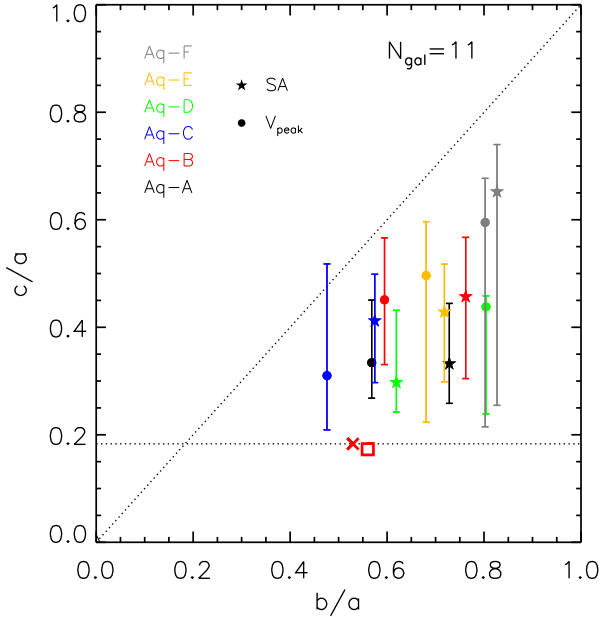


Figure 7. The axis ratios describing the shape of satellite systems in the Aquarius simulations and in the Milky Way. c/a is the minor to major axis ratio and b/a the intermediate to major axis ratio. Results for the top 11 satellites in the semi-analytic and V_{peak} models are shown by asterisks and filled circles respectively, with error bars spanning the range obtained for a large sample of satellites taking into account systematic effects introduced by the zone of avoidance (see text for details). The axis ratios for the 11 classical satellites of the Milky Way are shown with a red cross with the value of c/a highlighted by the horizontal dotted line. The average axis ratios of the 6 Aquarius dark matter halo (within r_{200}) are shown as the large open triangle towards the top-right corner. The red square shows the effect of including Canes Venatici in the observational sample.

proportional to the rms deviation of the x , y and z coordinates of the system. Denoting the major, intermediate and minor axes by a , b and c respectively ($a > b > c$), the flattening of the system may be quantified by the axial ratios c/a and b/a .

The axial ratios of the system consisting of the 11 classical satellites of the Milky Way are indicated by a red cross in Figs. 7 and 8, with the value of $c/a = 0.18$ highlighted by the horizontal dotted line. This is slightly lower than the value obtained by Libeskind et al. (2005) who had an error in their computer code (N. Libeskind, private communication). The faintest of the 11 classical satellites are Draco and Ursa Minor ($M_V = -8.8$), but Canes Venatici is just 0.2 mag fainter than this (McConnachie 2012). We have checked that including Canes Venatici has virtually no effect in the estimated axis ratios of the system, as shown by the red square in Fig. 7.

The corrected value of c/a for the Milky Way’s classical satellite appears quite extreme. However, with a sample of only 11 objects, it is not immediately obvious that a value even as low as $c/a = 0.18$ is significant. To assess the significance of this result, we follow Libeskind et al. (2005) and create a large number of artificial systems of 11 satellites

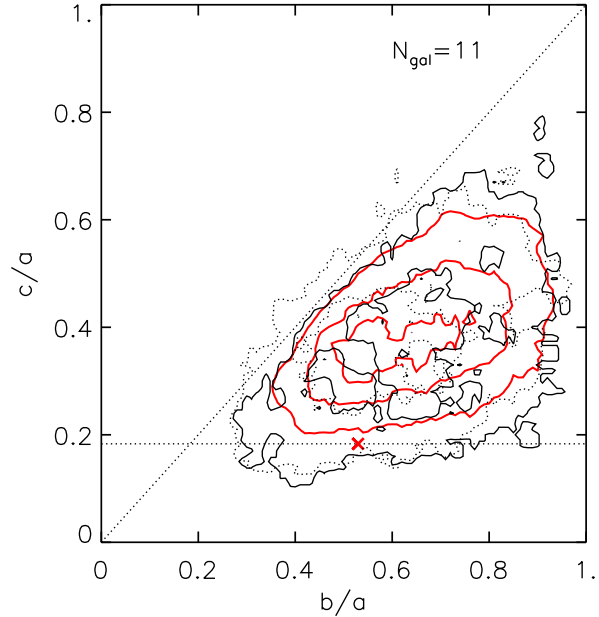


Figure 8. The distribution of shape parameters for systems of 11 satellites. The black lines show results for systems around 1686 Milky Way like halos in the MII and the dotted lines indicate the results after correcting for missing satellites in the galactic plane as described in the text. The red lines show results for 10000 randomly selected systems with the same radial distribution as the observed satellites of the Milky Way, but with a uniform distribution in solid angle. The three contour levels correspond to fractions of 30, 60 and 90 percent. The axis ratios of the 11 classical satellites of the Milky Way are indicated by the red cross, with the value of c/a highlighted by the horizontal dotted line.

in which the radial distances of the members are the same as the distances of the real satellites, but the latitude and longitude are assigned at random on the surface of a sphere. Isocontours of axial ratios for a set of 10,000 such isotropic systems, corresponding to number fractions of 30, 60 and 90 percent, are shown as red curves in Fig. 8. We find that only 98 of these samples result in values of c/a smaller than 0.18. Thus, we conclude that the distribution of the 11 classical satellites of the Milky Way is highly anisotropic, with only a 1 per cent probability that such a low value of c/a would result from a statistical fluctuation of an intrinsically isotropic system.

Applying the same procedure to the simulations we obtain the axis ratios for systems consisting of the top 11 satellites, ranked by stellar mass, that lie within 250 kpc of the centre in our two models. The results are shown in Fig. 7 for the six Aquarius halos, using asterisks for the semi-analytic model and circles for the V_{peak} model. We also plot the average axis ratios of the 6 Aquarius halos as a whole (within r_{200}) as a large triangle. The axis ratios of the 11 classical satellites of the Milky Way are plotted as a red cross. Three conclusions emerge from this figure. Firstly, as noted earlier by Libeskind et al. (2005) and Kang et al. (2005), massive satellite systems can be much flatter than the halo as a whole. Secondly, the two methods for ranking galaxies by

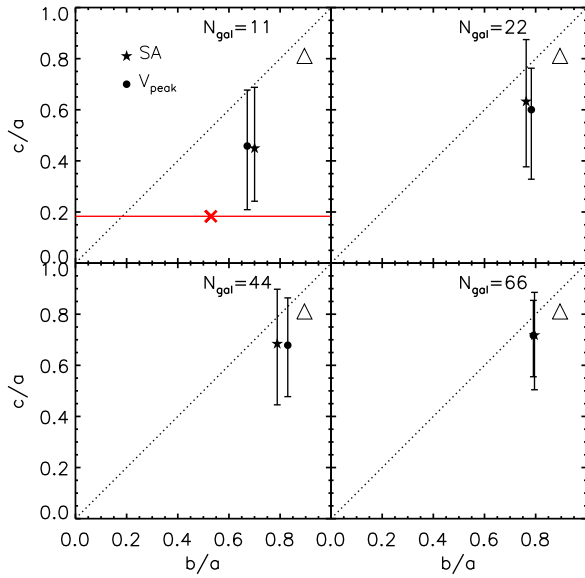


Figure 9. Shape parameters for systems consisting of the top N_{gal} satellites according to our two models of satellite galaxy formation. The symbols (asterisks for the semi-analytic model and filled circles for the V_{peak} model) give the directly measured mean values, averaged over the 6 Aquarius halos. The error bars span the minimum and maximum values amongst the 6 halos after correction for satellites missing due to obscuration in the Galactic plane. The four panels show results for $N_{\text{gal}} = 11, 22, 44,$ and 66 . In the top-left panel, the values for the top 11 satellites of the Milky Way ranked by luminosity are indicated by a red cross, with the value of c/a highlighted by a red horizontal solid line. The triangle near the top-right corner of each panel shows the mean axis ratios of the entire dark matter distribution in the 6 Aquarius halos.

stellar mass give very similar results. Thirdly, the satellite systems in the simulations appear generally less flattened than the 11 classical Milky Way satellites.

Although it is often assumed that the 11 classical satellites represent a complete sample of bright satellites in the central regions of the Milky Way, it is, of course, possible that bright satellites might remain undetected in the zone of avoidance as a result both of large extinction and confusion by foreground stars. Assuming that satellites are intrinsically uniformly distributed in $(1 - \sin|b|)$, where b denotes Galactic latitude, Willman et al. (2004) estimated that the known population of dwarf satellites could be 33 percent incomplete because of obscuration. However, Whiting et al. (2007) argued that, at most, there are one or two dwarfs still undiscovered near the Galactic plane.

To assess the possible effects of obscuration, we assume a geometry for the Galactic disk in our simulations and exclude satellites in the corresponding zone of avoidance. The “great pancake” in the Milky Way lies perpendicular to the Galactic disk. We therefore imagine that each of our Aquarius halos has a “Galactic plane” whose normal is parallel to the major axis of its satellite system. We then calculate the latitude of each satellite relative to this plane. If the latitude

is less than a critical value, $\pm\theta_{\text{crit}}$, we regard this satellite as undetected and exclude it from our sample of 11, replacing it by the next in the list. (For a 33 percent occulted sky fraction, $\theta_{\text{crit}} = 9.5^\circ$.) We repeat this process iteratively 2000 times, each time recalculating the shape of the current satellite system and the position of the obscuring “Galactic plane.” In 2000 cases, satellites were hidden behind the model galactic plane and replaced, on average, with 2.6 new satellites.

The results of this procedure, for $\theta_{\text{crit}} = 9.5^\circ$, are reflected in Fig. 7 as error bars spanning the range of c/a , with the uncorrected sample shown as a filled symbol. It is striking that the inferred shape of the satellite system is extremely sensitive to the inclusion or exclusion of only one or two members. Allowing for sample incompleteness improves the comparison between models and data noticeably, with several of the models now coming close to the data.

To improve our statistics, we also analysed satellite systems in the M_{RII}. As discussed earlier, the V_{peak} model is strongly affected by the relatively low resolution of the M_{RII}, but not so the semi-analytic model, provided satellites with dark matter haloes below the resolution limit are included in the analysis. As before, we consider all dark matter halos with virial mass $1 \times 10^{12} \leq M_{200} \leq 2 \times 10^{12}$ that have at least 11 satellites within 250 kpc. This provides a sample of 1686 Milky Way halos. The axis ratios of the brightest 11 satellites in each of the systems are shown as the black contours in Fig. 8, where levels correspond to number fractions of 30, 60 and 90 percent. We find only 101 satellite systems with an axis ratio c/a smaller than the observed value of 0.18, giving a probability of finding a configuration flatter than that in the MW of only $101/1686 = 6\%$.

Just as for the Aquarius sample, we make a correction for the possible omission of satellites near the Galactic disk. For each halo, we assume a Galactic plane perpendicular to the minor axis of the satellite distribution, draw 2000 random samples (replacing lost satellites and iterating) and obtain the mean values of the axis ratios. As the dotted contour in Fig 8 shows, the probability of finding a system in the simulations as flat or flatter than that of the Milky Way is not sensitive to our corrections for obscuration by the Galactic disk (under the assumption that the minor axes of the satellite system and the disk are perpendicular).

The high mass resolution of the Aquarius simulations allows us to investigate how the flattening of the satellite system varies as increasingly faint satellites are included in the sample and thus to make predictions for the larger samples that may become available in the future as surveys such as Pan-STARRS1 and LSST discover new, fainter satellites in the Milky Way. The axial ratios for systems of $N_{\text{gal}} = 11, 22, 44$ and 66 satellites are shown in the four panels of Fig. 9. The minimum and maximum values amongst the 6 Aquarius halos, after correcting for the effects of the zone of avoidance, as discussed above, are indicated by the error bars. Fig. 9 shows that, as the size of the satellite sample increases, the distribution becomes increasingly less flattened, in agreement with the results of Kang et al. (2005). When the sample size reaches 66, the shape of the satellite configuration is very close to that of halo dark matter, indicated by a large triangle in each panel. This prediction from our simulations should be readily testable with potentially

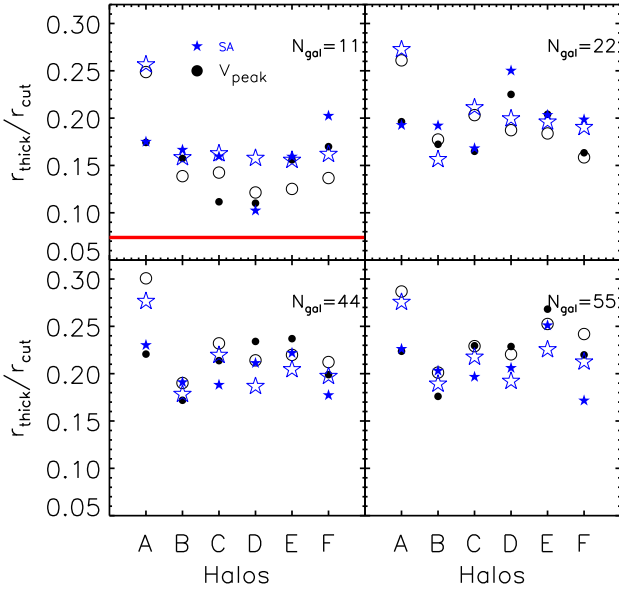


Figure 10. The flattening (defined as the ratio of the *rms* height of the satellites relative to the best fit plane divided by the radial extent of the system) of the satellite distribution in the six Aquarius halos. Different panels correspond to samples containing the top N_{gal} satellites according to our two models of satellite formation, which are illustrated by the filled symbols, as indicated in the legend. The open symbols show the average of 20,000 artificial samples each with the same radial distribution as the corresponding Aquarius sample but with random angular positions on the sky. In the $N_{\text{gal}} = 11$ panel the flattening of the 11 brightest satellites of the Milky Way, 0.074, is indicated by a red solid line.

forthcoming samples of new faint satellites, provided their selection functions are well understood.

3.2.2 The thickness of the satellite “disk”

An alternative method to estimate the flattening of the “Great pancake” is to measure the thickness of the slab defined by the pancake. Following Kroupa et al. (2005) and Kang et al. (2005), we find the best fit plane to a given satellite sample by minimizing the root-mean-square of the height of each satellite relative to the plane. The thickness of the slab is taken to be the *rms* height about the best-fit plane and the ratio of the thickness to the radial extent of the system, $R_{\text{cut}} = 250$ kpc, is used to characterise its flattening.

The flattening of the satellite disk in each of the six Aquarius halos is shown in Fig. 10. The four panels correspond to systems with different numbers of members, N_{gal} . Results for our two different satellite galaxy formation models are indicated by the filled symbols. The open symbols show results for 20,000 artificial samples with the same radial distribution as the corresponding Aquarius sample but with random angular positions on the sky. In some cases (e.g. Aq-A in all panels, Aq-D in the $N_{\text{gal}} = 11$ panel, Aq-C in the $N_{\text{gal}} = 22$ panel), the simulated satellite systems are signif-

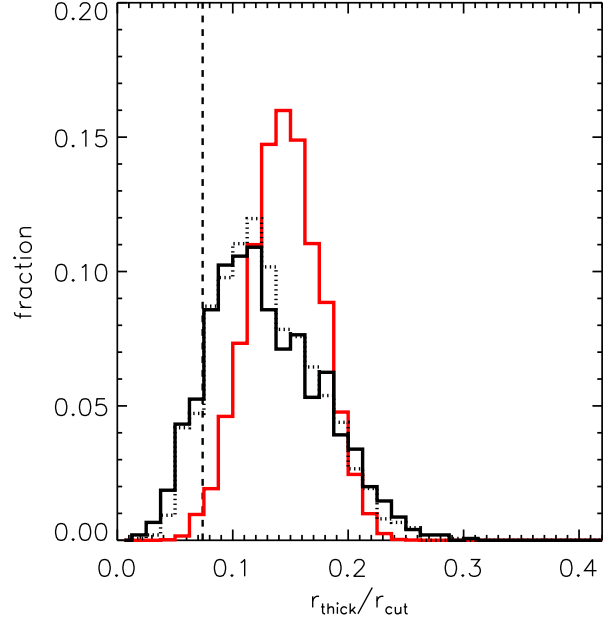


Figure 11. The distribution of flattenings (obtained from the *rms* height of satellites relative to the best-fit plane) for satellite systems. The solid black line shows results for the 1686 halos in the MR II with $1 \times 10^{12} \leq M_{200} \leq 2 \times 10^{12}$ that have at least 11 satellites within 250 kpc. The red histogram corresponds to 10000 samples with the same radial distribution as the 11 classical satellites of the Milky Way and a random distribution of angles on the sphere. The dotted histogram shows results for the MR II corrected for the possible loss of satellites near the Galactic disk taken from 2000 realizations. The flattening of the 11 classical satellites of the Milky Way, 0.074, is shown as a dashed vertical line.

icantly anisotropic but in others, the open symbols lie close to the filled symbols, indicating that these systems show no significant flattening according to this test. In the top left panel, we compare the model results with the measurement for the 11 classical satellites of the Milky Way, whose thickness (indicated by the red line) is 0.074. This population is clearly flatter than most of the simulations, although the satellite systems in Aq-C and Aq-D come close. The remaining panels in Fig. 10 show that, as was the case for the axial ratios, systems containing more and more satellites become progressively less flattened.

We also estimated the thickness of satellite systems in the 1686 Milky Way like halos found in the MR II as described in Section 3.2.1, which provides better statistics than the Aquarius halos. The histogram of flattening values is shown in Fig. 11. The value measured for the 11 classical satellites of the Milky Way, 0.074, is indicated by the vertical dashed line. This degree of flattening is highly significant: of 10000 artificial isotropic samples of 11 satellites having the same radial distribution as the observed satellites (red histogram), only 107 are flatter than the Milky Way system. This corresponds to a probability of only 1.07 percent. In the MR II a total of 219 cases have flatter satellite systems than the Milky Way, corresponding to a probability of 13 percent. When the effects of the Galactic disk are taken into

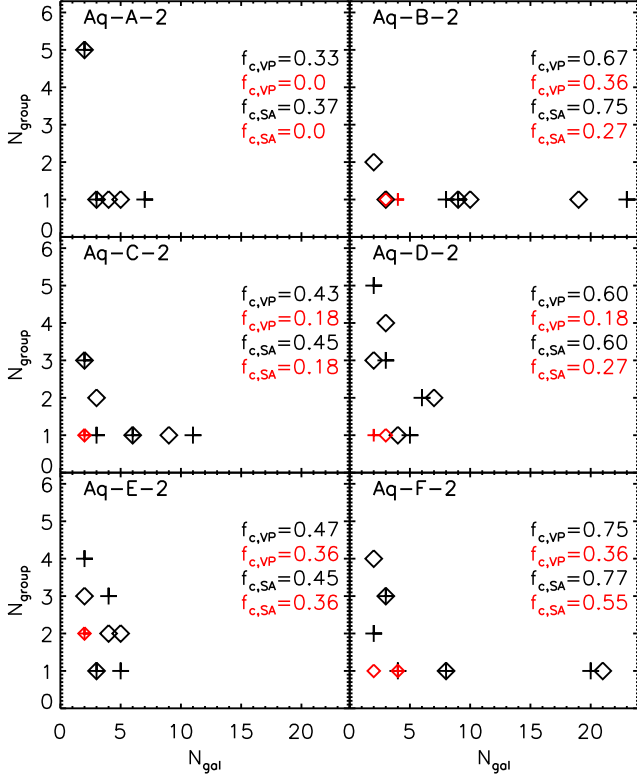


Figure 12. Histogram of multiple accretion satellite events in the six Aquarius halos. Satellites identified by the semi-analytic model are shown as diamonds, while those identified by the V_{peak} model are shown as crosses. In both cases, red symbols correspond to the top 11 satellites and black symbols to the top 60. The fractions of correlated halos relative to the total number of satellites, $f_{c,SA}(N)$, for the semi-analytic model, and $f_{c,VP}(N)$ for the V_{peak} model, where N is the number of satellites in the system, are given in the legend.

account, the distribution of flattenings is not significantly affected (dotted histogram in Fig. 11).

3.3 The multiplicity of accreted groups

As we have seen, the distribution of satellites in the Milky Way is significantly anisotropic. Libeskind et al. (2005) ascribed this striking property to the accretion of satellites along a few filaments of the cosmic web. However, in agreement with previous studies, we have shown that, although flattened satellite systems are common, the Milky Way’s satellites are even more flattened than the expectation for halos of similar mass. Li & Helmi (2008) noted that the natural flattening induced by this anisotropic infall is strongest when considering samples of galaxies accreted in ‘groups’, defined by common infall conditions (time, direction and orientation of orbital angular momentum). Considering all dark matter subhalos regardless of their mass, they found that samples of 11 subhalos drawn from only one such infalling ‘group’ have a configuration as flat as the classical Milky Way satellite distribution in 73 percent of cases. This probability falls to only 20 percent if only 5/11 satellites

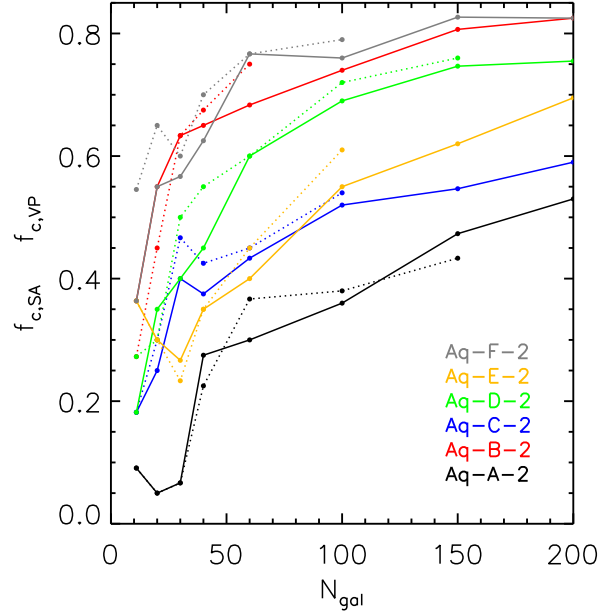


Figure 13. The fraction of the top N_{gal} satellites which are accreted into the main halo in a group with at least one partner, as a function of N_{gal} . The dotted lines show results for satellites in the semi-analytic model ($f_{c,SA}$), the solid lines for satellites in the V_{peak} model ($f_{c,VP}$).

are drawn from a single group. However, since Li & Helmi studied only one high-resolution halo, they were unable to quantify how likely it is that the *most massive* 11 satellites of the Milky Way fell in in just one or two groups and so to test whether or not this process is a probable explanation for their unusually flat configuration.

In order to explore the effect studied by Li & Helmi (2008) in our six ‘typical’ Milky Way halos, we identify satellites at the final time in the simulation and trace them back to the friends-of-friends group to which they belonged before they were accreted. If two or more satellites were part of the same group at one or more subsequent simulation snapshots, we regard them as correlated (Li & Helmi 2008 did not require their correlated subhalos to be members of the same FOF group, only to share similar infall times, directions and orbital angular momentum orientations; in practice the two definitions are likely to have similar results). In Fig. 12 we plot, for each Aquarius halo, the number of groups in which a given number of satellites were brought into the main halo (counting only satellites surviving to redshift zero). As before, we identify satellites using both our semi-analytic and V_{peak} models (indicated by diamonds and crosses respectively) and we consider samples of $N_{\text{gal}} = 11$ (red symbols) and $N_{\text{gal}} = 60$ (black symbols) satellites. The fractions of correlated halos relative to the total number of satellites ($f_{c,SA}$ for the semi-analytic model and $f_{c,VP}$ for the V_{peak} model) are given in the legend.

Focussing first on the top 11 satellites in each model (red symbols), we can see that, except in the semi-analytic model for halo F, fewer than half of these satellites are members of groups according to our definition; that is, more than

half are accreted singly into the main halo. This suggests that the probability of the top 11 satellites falling into the halo as members of only two or three groups is low; the moderate flattenings of the Aquarius satellite systems represent the typical outcome of anisotropic accretion, and are not enhanced by closer orbital associations between particular satellites. Testing whether or not the extreme flattening of the Milky Way’s system can be explained by the rare occurrence of a handful of ‘rich’ or ‘top heavy’ accretion events, as proposed by Li & Helmi (2008), will require a much larger suite of simulations comparable to Aquarius.

The prevalence of strongly correlated accretion increases as we consider larger satellite samples. For example, in halos B and F more than 15 of the top 60 satellites were part of a single group before accretion, as may be seen in Fig. 12. The increase in $f_{c,SA}$ and $f_{c,VP}$ with the size of the satellite sample is illustrated in Fig. 13 and is seen in both our methods for ranking satellites. For systems of only 10 satellites, the correlated fraction is $\sim 10 - 50$ per cent, but this rises to $\sim 30 - 80$ per cent for systems of 100 satellites. Our findings reinforce the conclusion of Lovell et al. (2011) that a more complete census of satellite motions in the Milky Way and M31 will reveal a significant fraction with common orbital planes.

4 CONCLUSION AND DISCUSSION

The spatial distribution of satellites in the Milky Way and other galaxies reflects both the nature of the dark matter and the processes of galaxy formation. In this paper we have used high mass resolution cosmological simulations of structure formation in the Λ CDM model: the Aquarius resimulations of galactic scale dark matter halos and the Millennium II simulation (MII) of a cubic volume $100 h^{-1}\text{Mpc}$ on a side, with about 2000 halos of mass comparable to the Milky Way’s halo. We have further employed two models of galaxy formation to trace satellites in the simulation: the semi-analytic models of Cooper et al. (2010) and Guo et al. (2011) for Aquarius and MII respectively and a less sophisticated model in which galaxy stellar mass is assumed to be proportional to V_{peak} , the highest circular velocity attained by the halo throughout its life. Our two methods place 10 of the most massive 11 satellites in the same Aquarius halos.

The combination of high-resolution simulations and robust galaxy formation models allows us to identify satellites in a reliable way. We find that good mass resolution is essential to obtain an accurate estimate of the radial distribution of satellites. Indeed, even at the resolution of the MII, $m_p = 6.9 \times 10^6 h^{-1} M_\odot$, many genuine substructures are artificially destroyed, as may be seen in Fig. 5. In this case, the V_{peak} method for assigning stellar mass to satellites, as well as all previous cosmological simulations which have poorer resolution (e.g. Libeskind et al. 2005; Kang et al. 2005), would give inaccurate results. By contrast, our semi-analytic model, which continues to track satellites even after they have lost their halos does give a faithful prediction of the theoretical expectations in the Λ CDM model. In the case of the Aquarius simulations, the resolution is good enough that galaxies with unresolved halos are unimportant (Font et al. 2011) and we can

compare our semi-analytic results with the V_{peak} method. The results from the two ranking methods agree well.

Our main results concerning the satellite radial distribution are: (i) there is substantial halo-to-halo scatter in the radial distribution of satellites in the Aquarius simulations, but in all cases the massive satellites have a similar radial density profile to that of the dark matter; (ii) both the semi-analytic and V_{peak} models give results in good agreement with the measured radial distribution of the 11 classical satellites of the Milky Way; (iii) the radial density profile of larger satellite samples, going down to lower masses, is similar to that of the 11 most massive, at least up to samples of 100 satellites. This prediction may be tested by future surveys such as Pan-STARRS.

We also investigated the angular distribution of satellites. This is interesting because the Milky Way’s 11 brightest satellites show a very anisotropic distribution, the “Great pancake” of Libeskind et al. (2005). We characterized the angular distribution by measuring both the axial ratios of the satellite system and the thickness of the slab in which the satellites are concentrated. We verified that the peculiar distribution seen in the Milky Way is highly significant: only 1 percent of isotropic samples with the same radial distribution are flatter than the Milky Way’s system. In the 1686 halos in the MII which have a mass plausibly similar to that of the Milky Way we find systems flatter than that of the classical satellites with probabilities of 6 and 13 percent according to the axial ratio and slab thickness tests respectively. These probabilities are slightly lower than that found by Libeskind et al. (2005), who used a slightly incorrect value for the flattening of the Milky Way satellites. Our probabilities are also lower than those found by Kang et al. (2005), a discrepancy that is readily understood as a consequence of the poor mass resolution of the simulations used by these authors. The Milky Way system thus appears to be in the tail of the flattening distribution expected for massive satellites in the Λ CDM model. The presence of a satellite as massive as the LMC (Boylan-Kolchin et al. 2010; Busha et al. 2011; Guo et al. 2011; Liu et al. 2011) and the polar alignment of the system (Deason et al. 2011) seem to be comparably rare, but still consistent with the predicted distributions.

Finally, we investigated the extent to which satellites are accreted in groups. This is interesting for several reasons, including the possibility that the Great pancake might be explained by multiple accretion in 2-3 groups (Li & Helmi 2008). Our simulations confirm that this is a rare occurrence in Λ CDM. On average, only 30 percent of the top 11 satellites in the Aquarius simulations share a friends-of-friends group with another top 11 satellite before infall; the rest come into the main halo without any companions of comparable mass. However, multiple accretion becomes increasingly important for larger, fainter samples of satellites. For example, in samples of the 60 most massive satellites in two of the Aquarius halos (Aq-B and Aq-F), we find that as many as 20 come into the main halo in a single group and as many as 11 in the other simulated halos. This interesting property may potentially have observational consequences (e.g. Sales et al. 2011).

Libeskind et al. (2005) proposed that filamentary accretion is responsible for the flattening of Milky Way-like satellite populations. Lovell et al. (2011) subsequently

showed that the subhalos of the Aquarius simulations have strongly correlated orbital angular momenta as the result of anisotropic accretion. Recently, however, Pawlowski et al. (2012) re-analysed the angular momentum orientations of subhalos in Aquarius (as presented in Lovell et al. 2011) and concluded that anisotropic accretion is unimportant for producing flattened satellite systems, in direct contradiction with the results of Libeskind et al. (2005) and Lovell et al. (2011). They required that the Milky Way flattening should be reproduced in the mean, rather than being merely consistent with the expected distribution. As the Milky Way is in the ~ 10 per cent tail of the distribution predicted by Λ CDM (as our study and others have shown), they reject a CDM model in favour of tidal galaxy formation, which they claim readily produces highly correlated disks of satellites. We believe that the explanation offered by Libeskind et al. (2005) remains the most appropriate. A single randomly chosen system such as the Milky Way is extremely unlikely perfectly to represent the mean value of every measurable property. A larger sample of satellites around other galaxies will test the tidal formation hypothesis of Pawlowski et al. (2012) in which highly flattened configurations are easily achieved and should therefore be the norm. If, on the other hand, the CDM model is a realistic description of nature, then the average satellite configurations should be only moderately flattened, as illustrated in Figs. 7 and 8.

Our simulations are useful not only to test our models against data for the classical satellites of the Milky Way, as we have done here, but also to make predictions for future surveys that will quantify the spatial distribution of larger and fainter satellite samples, both in the Milky Way and in other galaxies. For a sample of Milky Way satellites complete to very faint magnitudes, we have shown that the luminosity function (Font et al. 2011), radial distribution and system shape should vary less from halo to halo than is the case for the most massive eleven. Measuring these three highly characteristic properties of the satellite system test both the Λ CDM cosmology and models of galaxy formation in novel, interesting ways.

ACKNOWLEDGEMENTS

We thank Julio Navarro and Simon White for useful suggestions and comments, and Qi Guo for useful discussions and explanation of the MR11 galaxy catalogue. The simulations of the Aquarius Project were carried out at the Leibniz Computing Center, Garching, Germany, at the Computing Centre of the Max-Planck-Society in Garching, at the Institute for Computational Cosmology in Durham, and on the ‘STELLA’ supercomputer of the LOFAR experiment at the University of Groningen. JW acknowledges a Royal Society Newton International Fellowship, CSF a Royal Society Wolfson Research Merit Award and ERC Advanced Investigator grant, COSMIWAY. This work was supported by an STFC rolling grant to the Institute for Computational Cosmology.

This paper has been typeset from a \LaTeX file prepared by the author.

REFERENCES

- Benson A. J., Frenk C. S., Lacey C. G., Baugh C. M., Cole S., 2002, *MNRAS*, 333, 177
- Boylan-Kolchin M., Springel V., White S. D. M., Jenkins A., 2010, *MNRAS*, 406, 896
- Boylan-Kolchin M., Springel V., White S. D. M., Jenkins A., Lemson G., 2009, *MNRAS*, 398, 1150
- Bullock J. S., Kravtsov A. V., Weinberg D. H., 2000, *ApJ*, 539, 517
- Busha M. T., Alvarez M. A., Wechsler R. H., Abel T., Strigari L. E., 2010, *ApJ*, 710, 408
- Busha M. T., Wechsler R. H., Behroozi P. S., Gerke B. F., Klypin A. A., Primack J. R., 2011, *ApJ*, 743, 117
- Cooper A. P., Cole S., Frenk C. S., White S. D. M., Helly J., Benson A. J., De Lucia G., Helmi A., Jenkins A., Navarro J. F., Springel V., Wang J., 2010, *MNRAS*, 406, 744
- Crain R. A., Theuns T., Dalla Vecchia C., Eke V. R., Frenk C. S., Jenkins A., Kay S. T., Peacock J. A., Pearce F. R., Schaye J., Springel V., Thomas P. A., White S. D. M., Wiersma R. P. C., 2009, *MNRAS*, 399, 1773
- Davis M., Efstathiou G., Frenk C. S., White S. D. M., 1985, *ApJ*, 292, 371
- Deason A. J., McCarthy I. G., Font A. S., Evans N. W., Frenk C. S., Belokurov V., Libeskind N. I., Crain R. A., Theuns T., 2011, *MNRAS*, 415, 2607
- Diemand J., Kuhlen M., Madau P., 2007, *ApJ*, 667, 859
- Font A. S., Benson A. J., Bower R. G., Frenk C. S., Cooper A., De Lucia G., Helly J. C., Helmi A., Li Y.-S., McCarthy I. G., Navarro J. F., Springel V., Starkenburg E., Wang J., White S. D. M., 2011, *MNRAS*, 417, 1260
- Guo Q., Cole S., Eke V., Frenk C., 2011, *MNRAS*, 417, 370
- Guo Q., White S., Boylan-Kolchin M., De Lucia G., Kauffmann G., Lemson G., Li C., Springel V., Weinmann S., 2011, *MNRAS*, 413, 101
- Kaiser N., Burgett W., Chambers K., Denneau L., Heasley J., Jedicke R., Magnier E., Morgan J., Onaka P., Tonry J., 2010, in *Society of Photo-Optical Instrumentation Engineers (SPIE) Conference Series Vol. 7733 of Society of Photo-Optical Instrumentation Engineers (SPIE) Conference Series, The Pan-STARRS wide-field optical/NIR imaging survey*
- Kang X., Mao S., Gao L., Jing Y. P., 2005, *A&A*, 437, 383
- Koposov S. E., Yoo J., Rix H.-W., Weinberg D. H., Macciò A. V., Escudé J. M., 2009, *ApJ*, 696, 2179
- Kravtsov A. V., Gnedin O. Y., Klypin A. A., 2004, *ApJ*, 609, 482
- Kroupa P., Theis C., Boily C. M., 2005, *A&A*, 431, 517
- Kunkel W. E., 1979, *ApJ*, 228, 718
- Li Y.-S., De Lucia G., Helmi A., 2010, *MNRAS*, 401, 2036
- Li Y.-S., Helmi A., 2008, *MNRAS*, 385, 1365
- Libeskind N. I., Frenk C. S., Cole S., Helly J. C., Jenkins A., Navarro J. F., Power C., 2005, *MNRAS*, 363, 146
- Libeskind N. I., Frenk C. S., Cole S., Jenkins A., Helly J. C., 2009, *MNRAS*, 399, 550
- Liu L., Gerke B. F., Wechsler R. H., Behroozi P. S., Busha M. T., 2011, *ApJ*, 733, 62
- Lovell M. R., Eke V. R., Frenk C. S., Jenkins A., 2011, *MNRAS*, 413, 3013
- Lynden-Bell D., 1976, *MNRAS*, 174, 695
- Lynden-Bell D., 1982, *The Observatory*, 102, 202
- Macciò A. V., Kang X., Fontanot F., Somerville R. S., Ko-

- posov S., Monaco P., 2010, MNRAS, 402, 1995
- Martin N. F., McConnachie A. W., Irwin M., Widrow L. M., Ferguson A. M. N., Ibata R. A., Dubinski J., Babul A., Chapman S., Fardal M., Lewis G. F., Navarro J., Rich R. M., 2009, ApJ, 705, 758
- Mateo M. L., 1998, ARA&A, 36, 435
- McConnachie A. W., 2012, ArXiv e-prints
- McConnachie A. W., Irwin M. J., Ibata R. A., Dubinski J., Widrow L. M., Martin N. F., Côté P., Dotter A. L. e. a., 2009, Nature, 461, 66
- Muñoz J. A., Madau P., Loeb A., Diemand J., 2009, MNRAS, 400, 1593
- Navarro J. F., Ludlow A., Springel V., Wang J., Vogelsberger M., White S. D. M., Jenkins A., Frenk C. S., Helmi A., 2010, MNRAS, 402, 21
- Okamoto T., Frenk C. S., Jenkins A., Theuns T., 2010, MNRAS, 406, 208
- Parry O. H., Eke V. R., Frenk C. S., Okamoto T., 2012, MNRAS, 419, 3304
- Pawlowski M. S., Kroupa P., Angus G., de Boer K. S., Famaey B., Hensler G., 2012, ArXiv e-prints
- Sales L. V., Navarro J. F., Cooper A. P., White S. D. M., Frenk C. S., Helmi A., 2011, MNRAS, 418, 648
- Somerville R. S., 2002, ApJ, 572, L23
- Spergel D. N., Verde L., Peiris H. V., Komatsu E., Nolta M. R., Bennett C. L., Halpern M., Hinshaw G., Jarosik N., Kogut A., Limon M., Meyer S. S., Page L., Tucker G. S., Weiland J. L., Wollack E., Wright E. L., 2003, ApJS, 148, 175
- Springel V., Wang J., Vogelsberger M., Ludlow A., Jenkins A., Helmi A., Navarro J. F., Frenk C. S., White S. D. M., 2008, MNRAS, 391, 1685
- Springel V., White S. D. M., Jenkins A., Frenk C. S., Yoshida N., Gao L., Navarro J., Thacker R., Croton D., Helly J., Peacock J. A., Cole S., Thomas P., Couchman H., Evrard A., Colberg J., Pearce F., 2005, Nature, 435, 629
- Stoehr F., White S. D. M., Tormen G., Springel V., 2002, MNRAS, 335, L84
- Wadepuhl M., Springel V., 2011, MNRAS, 410, 1975
- Wang J., Frenk C. S., Navarro J. F., Gao L., Sawala T., 2012, ArXiv e-prints
- Wang J., Navarro J. F., Frenk C. S., White S. D. M., Springel V., Jenkins A., Helmi A., Ludlow A., Vogelsberger M., 2011, MNRAS, 413, 1373
- Whiting A. B., Hau G. K. T., Irwin M., Verdugo M., 2007, AJ, 133, 715
- Willman B., Governato F., Dalcanton J. J., Reed D., Quinn T., 2004, MNRAS, 353, 639
- Zentner A. R., Kravtsov A. V., Gnedin O. Y., Klypin A. A., 2005, ApJ, 629, 219